# 11β-HSD1 is the major regulator of the tissue-specific effects of circulating glucocorticoid excess

Stuart A. Morgan[a], Emma L. McCabe[a,1], Laura L. Gathercole[a,1], Zaki K. Hassan-Smith[a], Dean P. Larner[a], Iwona J. Bujalska[a], Paul M. Stewart[a,b,2], Jeremy W. Tomlinson[a,2,3], and Gareth G. Lavery[a,2]

[a]Centre for Endocrinology, Diabetes and Metabolism, School of Clinical and Experimental Medicine, Institute of Biomedical Research, University of Birmingham, Birmingham B15 2TT, United Kingdom; and [b]School of Medicine, University of Leeds, Leeds LS2 9JT, United Kingdom

Edited by Jan-Åke Gustafsson, University of Houston, Houston, Texas, and approved May 1, 2014 (received for review December 28, 2013)

**The adverse metabolic effects of prescribed and endogenous glucocorticoid (GC) excess, Cushing syndrome, create a significant health burden. We found that tissue regeneration of GCs by 11β-hydroxysteroid dehydrogenase type 1 (11β-HSD1), rather than circulating delivery, is critical to developing the phenotype of GC excess; 11β-HSD1 KO mice with circulating GC excess are protected from the glucose intolerance, hyperinsulinemia, hepatic steatosis, adiposity, hypertension, myopathy, and dermal atrophy of Cushing syndrome. Whereas liver-specific 11β-HSD1 KO mice developed a full Cushingoid phenotype, adipose-specific 11β-HSD1 KO mice were protected from hepatic steatosis and circulating fatty acid excess. These data challenge our current view of GC action, demonstrating 11β-HSD1, particularly in adipose tissue, is key to the development of the adverse metabolic profile associated with circulating GC excess, offering 11β-HSD1 inhibition as a previously unidentified approach to treat Cushing syndrome.**

endocrinology | cortisol | HSD11b1 | hypercortisolemia | steroids

Estimates suggest that 1–2% of the population of the United States and United Kingdom take prescribed glucocorticoids (GCs) for the treatment of a broad spectrum of inflammatory and autoimmune diseases (1, 2). Despite the efficacy of GCs, 70% of patients experience an adverse systemic side-effect profile. The resultant Cushingoid features include central obesity, proximal myoatrophy, hypertension, skin thinning, osteoporosis, hepatic steatosis, insulin resistance, and type 2 diabetes (3, 4). Collectively, this contributes to increased risk of cardiovascular morbidity and mortality (5, 6). These features are replicated in patients with much rarer endogenous GC excess (Cushing syndrome), as first described by Harvey Cushing in 1932 (7). Current medical therapeutic options that reverse the tissue-specific consequences of hypercortisolism are limited.

GC availability and action depend not only upon circulating levels but also on tissue-specific intracellular metabolism by 11β-hydroxysteroid dehydrogenases (11β-HSDs). Key metabolic tissues including liver, adipose tissue, and skeletal muscle express 11β-HSD type 1 (11β-HSD1), which coverts inactive cortisone to active cortisol [11-dehydrocorticosterone (11DHC) and corticosterone (CORT) in rodents, respectively] (8). In the setting of GC excess, the relative contribution to the metabolic effects induced by GCs of simple delivery of active GCs (cortisol or CORT) to a target tissue, compared with the regeneration of active GCs by 11β-HSD1 within the tissue, has not been determined.

Type 2 11β-HSD (11β-HSD2) is predominately expressed in the kidney, colon, and salivary gland and catalyzes the inactivation of cortisol to cortisone (CORT to 11DHC in rodents). This not only protects the mineralocorticoid receptor from occupancy by cortisol but also crucially provides substrate for 11β-HSD1 in peripheral tissues.

Transgenic animal models have highlighted the critical role of 11β-HSD1 in the regulation of metabolic phenotype in individual tissues. Mice overexpressing 11β-HSD1, specifically in adipose tissue, develop visceral obesity, insulin resistance, dyslipidemia, and hypertension (9, 10). Similarly, liver-specific 11β-HSD1 overexpression results in insulin resistance and hypertension, but not obesity (11). Importantly, circulating CORT levels were not elevated in either model, suggesting increased intracellular GC availability underpins the observed phenotypes. Indeed, this was confirmed in the adipose-specific 11β-HSD1–overexpressing mice, where twofold higher intraadipose CORT levels were recorded in comparison with WT controls (9). Ultimately, this has led to the development of selective 11β-HSD1 inhibitors as a potential treatment for patients with diabetes, obesity, and hypertension (12, 13).

Although it is clear that 11β-HSD1 has a critical role to play in governing GC availability, its potential dynamic role in the setting of GC excess has not been fully explored (14–16). We have previously reported a patient with Cushing disease who was protected from the classic Cushing phenotype, owing to a functional defect in 11β-HSD1 activity, as evidenced by serum and urinary biomarkers (17). Based on this observation, we have hypothesized that tissue intrinsic 11β-HSD1 activity is the major determinant of the manifestations of GC excess and that 11β-HSD1 deletion will ameliorate the associated metabolic abnormalities. To determine the relative tissue-specific contribution to this effect, we have generated tissue-specific 11β-HSD1 deletions in liver and adipose tissue.

## Significance

**Glucocorticoids are widely prescribed for their anti-inflammatory properties but have Cushingoid side effects that contribute significantly to patient morbidity and mortality. Here we present data to demonstrate that the adverse side-effect profile associated with exogenous active glucocorticoid (GC) administration (including glucose intolerance, hyperinsulinemia, hypertension, hepatic steatosis, increased adiposity, and myopathy) is prevented by global deletion of 11β-hydroxysteroid dehydrogenase type 1 (11β-HSD1) in mice. This study not only defines a significant shift in our understanding of the physiological and molecular mechanisms underpinning the adverse side effects associated with GC use but also raises the possibility of targeting 11β-HSD1 as a novel adjunctive therapy in the treatment of Cushing syndrome.**

Author contributions: S.A.M., J.W.T., and G.G.L. designed research; S.A.M., E.L.M., L.L.G., Z.K.H.-S., and D.P.L. performed research; P.M.S., J.W.T., and G.G.L. contributed new reagents/analytic tools; S.A.M. and I.J.B. analyzed data; and S.A.M., P.M.S., J.W.T., and G.G.L. wrote the paper.

The authors declare no conflict of interest.

This article is a PNAS Direct Submission.

Freely available online through the PNAS open access option.

[1]E.L.M. and L.L.G. contributed equally to this work.

[2]P.M.S., J.W.T., and G.G.L. contributed equally to this work.

[3]To whom correspondence should be addressed. E-mail: j.w.tomlinson@bham.ac.uk.

This article contains supporting information online at www.pnas.org/lookup/suppl/doi:10.1073/pnas.1323681111/-/DCSupplemental.

## Results

**A Model of Exogenous GC Excess.** CORT treatment increased circulating CORT levels to a similar extent in both WT and 11β-HSD1 KO (GKO) animals, suggesting that all of the observations described below were independent of circulating active GC concentrations (Fig. 1*A*). This was associated with suppression of the hypothalamic–pituitary–adrenal axis and endogenous GC production, as indicated by adrenal atrophy in both WT mice and GKO mice (Fig. 1*B*).

**GKO Mice Are Protected from the Development of CORT-Induced Cushing Syndrome.** A schematic diagram demonstrating the central role 11β-HSD1 plays in governing intracellular access to circulating CORT is shown in Fig. 1*C*. The GC dose used in this study did not affect total body weight. WT mice treated with CORT were glucose-intolerant (Fig. 2 *A* and *B*), hyperinsulinemic (Fig. 2*C*), and hyperglycemic following a 5-h fast (Fig. 2*D*) and had a lower homeostatic model assessment as an index of insulin resistance (HOMA-IR) (Fig. 2*E*). Systolic blood pressure was also

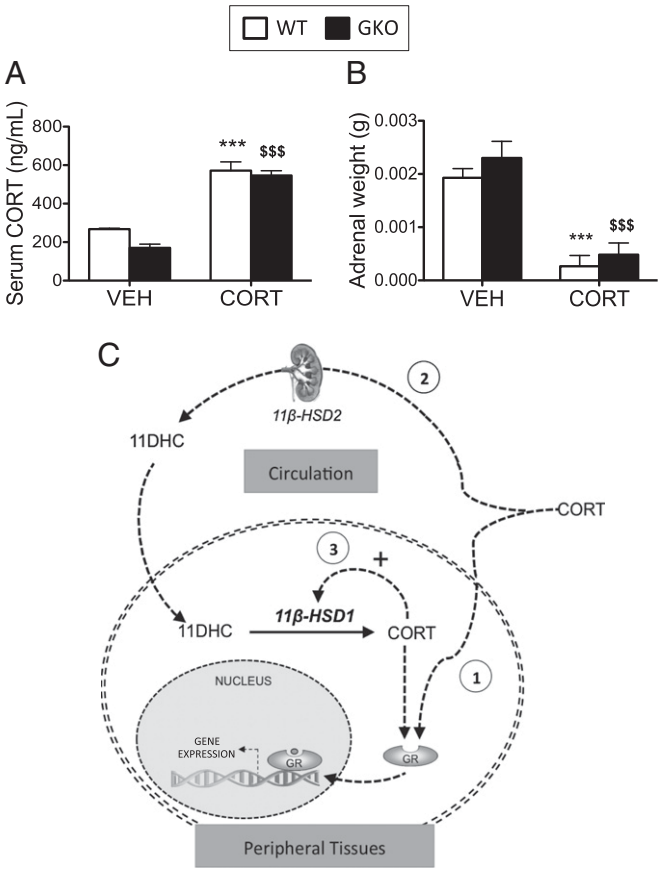


**Fig. 1.** WT and 11β-HSD1 KO mice administered CORT via the drinking water results in elevated circulating CORT levels. C57BL/6 WT (white bars) and 11β-HSD1 KO mice (GKO, black bars) were treated with CORT (100 μg/mL) or vehicle via the drinking water for 5 wk ($n$ = 7–9 in each group). Elevated circulating CORT (*A*) and suppressed adrenal weights (*B*) were observed in both CORT-treated WT and GKO mice. Data were analyzed using two-way ANOVA; see Fig. S1 for the complete dataset used in the analysis. $^{***}P < 0.001$ vs. WT vehicle; $^{\$\$\$}P < 0.001$ vs. GKO vehicle. (*C*) Schematic diagram summarizing the three mechanisms by which circulating CORT results in GR activation: (1) direct binding of circulating CORT with the GR in peripheral tissues; (2) inactivation of circulating CORT by 11β-HSD2, then reactivation in peripheral tissues by 11β-HSD1; and (3) GR activation increases 11β-HSD1 expression and activity, further amplifying intracellular CORT availability.

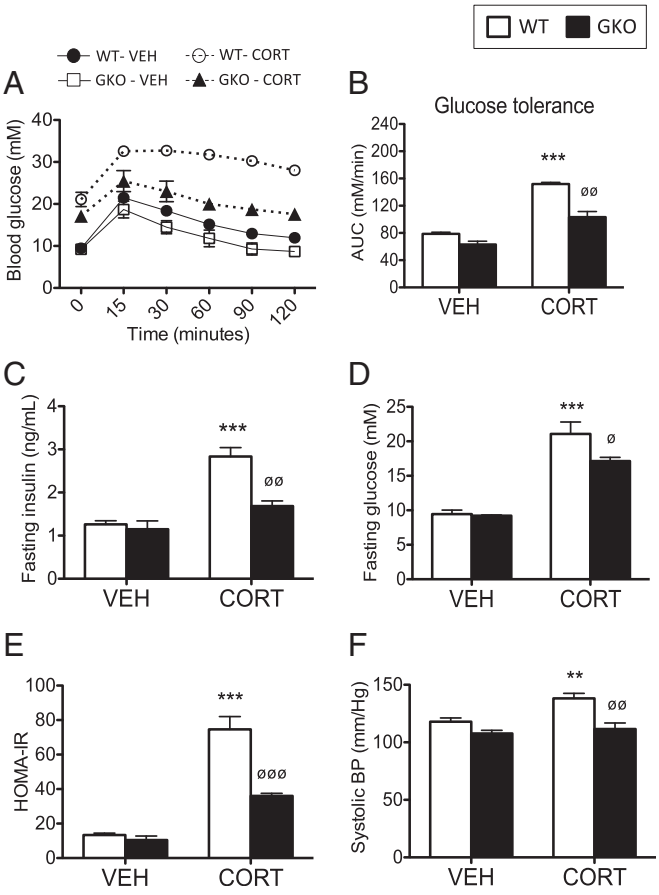


**Fig. 2.** Deletion of 11β-HSD1 ameliorates the adverse metabolic side-effect profile induced by CORT. C57BL/6 WT (white bars) and 11β-HSD1 KO mice (GKO, black bars) were treated with CORT (100 μg/mL) or vehicle via the drinking water for 5 wk ($n$ = 7–9 in each group). Glucose tolerance (*A*), calculated area under the curve (AUC) for glucose tolerance data (*B*), fasting insulin levels (*C*), fasting glucose (*D*), HOMA-IR index (*E*), and systolic blood pressure (BP) (*F*) were improved in CORT-treated GKO mice compared with CORT-treated WTs. Data were analyzed using two-way ANOVA; see Fig. S1 for the complete dataset used in the analysis. $^{**}P < 0.01$, $^{***}P < 0.001$ vs. WT vehicle; $^{ø}P < 0.05$, $^{øø}P < 0.01$, $^{ø ø ø}P < 0.001$ vs. WT CORT.

increased (Fig. 2*F*). In contrast, CORT-treated GKO mice remained relatively glucose-tolerant (Fig. 2 *A* and *B*), had lower fasting insulin and glucose levels (Fig. 2 *C* and *D*) and an improved HOMA-IR index (Fig. 2*E*), no change in systolic blood pressure (Fig. 2*F*), and were therefore protected from the adverse effects of systemic GC excess.

**Liver.** Nonalcoholic fatty liver disease is a common feature of GC excess in humans. Consistent with this, WT mice had increased hepatic triglyceride (TAG) content following CORT treatment, as demonstrated by oil red O staining (Fig. 3*A*). This was endorsed using a quantitative TAG assay (Fig. 3*B*). Serum free fatty acid levels were also increased (Fig. 3*C*), paralleled by elevated expression of CD36 (a membrane protein that facilitates fatty acid uptake) (Fig. 3*D*) in WT mice following CORT treatment. By contrast, GKO mice were completely protected from CORT-induced hepatic steatosis (Fig. 3 *A* and *B*), increased serum free fatty acid levels (Fig. 3*C*), and increased hepatic CD36 expression (Fig. 3*D*). The mRNA expression of the key hepatic lipogenic enzymes, acetyl-coA carboxylase 1 (ACC1), fatty acid synthase (FAS), and diacylglycerol acyltransferase-1 (DGAT1), and transcription factors regulating lipogenesis, peroxisome proliferator-activated receptor-gamma (PPARG) and cAMP

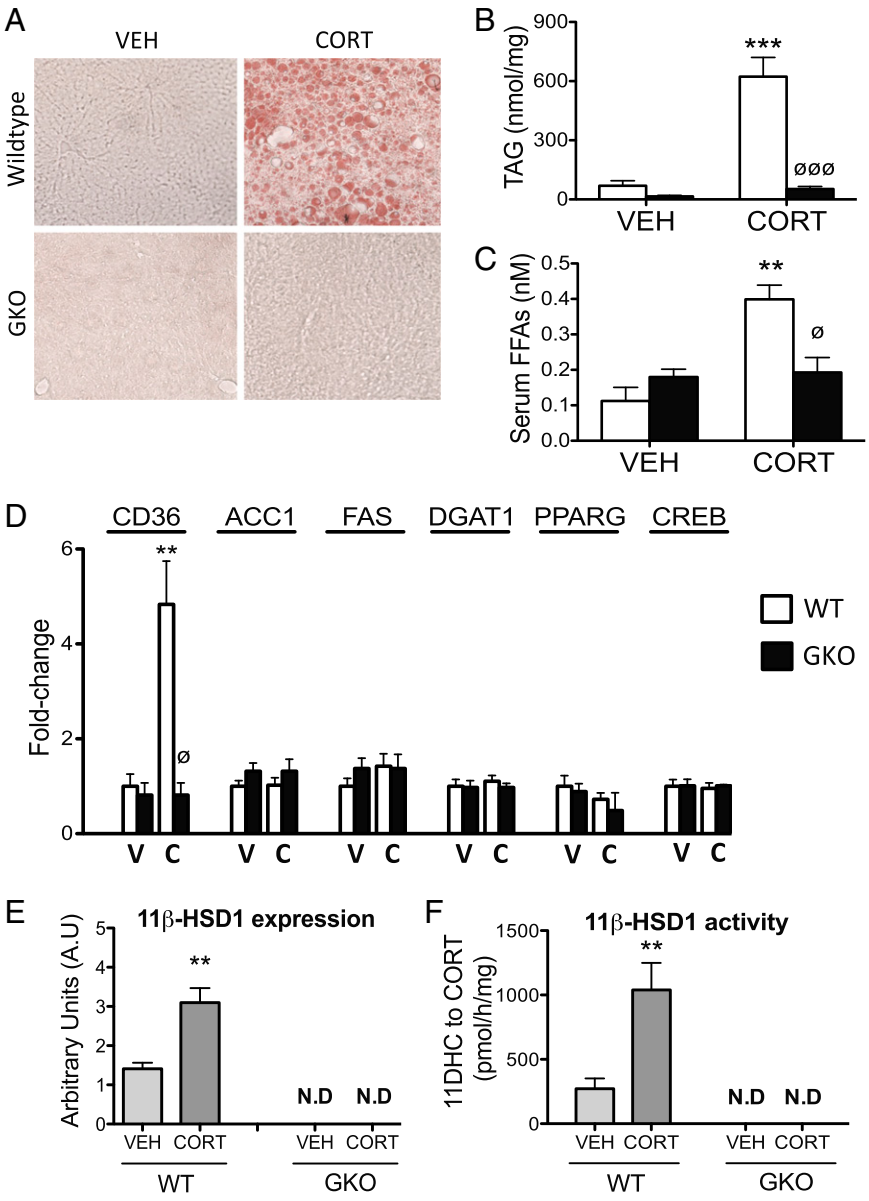


**Fig. 3.** The 11β-HSD1 KO mice are protected from the development of CORT-induced hepatic steatosis. Frozen liver sections stained with oil red O (*A*) and a quantitative TAG assay (*B*) revealed 11β-HSD1 KO (GKO) mice were protected from CORT-induced hepatic steatosis. GKO mice were also protected from increased serum free fatty acids (*C*) and increased haptic mRNA expression of CD36 (*D*) induced by CORT. The expression of the key lipogenic modulators in the liver, ACC1, FAS, DGAT1, PPARG, and CREB, was unaffected by CORT in both WT and GKO mice (*D*). Data were analyzed using two-way ANOVA; see Fig. S2 for the complete dataset used in the analysis. Hepatic 11β-HSD1 mRNA expression (*E*) and oxo-reductase activity (*F*) were increased following CORT treatment in WT mice but not GKO mice. Data were analyzed using Student *t* tests ($n$ = 7–9 in each group). $^{**}P < 0.01$, $^{***}P < 0.001$ vs. WT vehicle; $^{\varnothing}P < 0.05$, $^{\varnothing\varnothing\varnothing}P < 0.001$ vs. WT CORT. C, CORT; N.D, not detected; V, vehicle.

response element-binding protein (CREB), were unaffected by CORT treatment in both WT and GKO mice (Fig. 3*D*). These data suggest that increased lipid delivery and uptake are likely to be the major contributing factor to GC-induced hepatic steatosis in WT mice. Consistent with our hypothesis that GC excess acts as a "feed-forward" signal to increase intracellular CORT availability, 11β-HSD1 mRNA expression and 11β-HSD1–mediated oxo-reductase activity (conversion of 11DHC to CORT) was increased in the liver of CORT-treated WT mice compared with vehicle-treated controls. By contrast, no 11β-HSD1 expression or oxo-reductase activity was detected in the liver of either vehicle- or CORT-treated GKO mice, confirming that no alternative reductase is capable of compensating for deletion of 11β-HSD1 (Fig. 3 *E* and *F*).

**Adipose Tissue.** Increased adiposity, particularly in visceral depots, is a well-characterized feature associated with GC excess. Gonadal, mesenteric, retroperitoneal, and s.c. adipose tissue depot weights were increased in WT mice following CORT treatment (Fig. 4 *A*–*D*). By contrast, CORT-treated GKO mice were protected from this increase (Fig. 4 *A*–*D*). Adipocyte size was increased in both gonadal (Fig. 4 *E* and *G*) and s.c. depots (Fig. 4*F*) of CORT-treated WT mice. CORT-treated GKO mice were not protected from increased adipocyte size in either depot, suggesting the observed decrease in fat pad weights was due to a reduction in adipocyte number (Fig. 4 *E*–*G*).

Gene expression analysis revealed increased expression of DGAT1 and the insulin signaling component insulin receptor substrate 2 (IRS2) in CORT-treated WT mice, suggesting increased

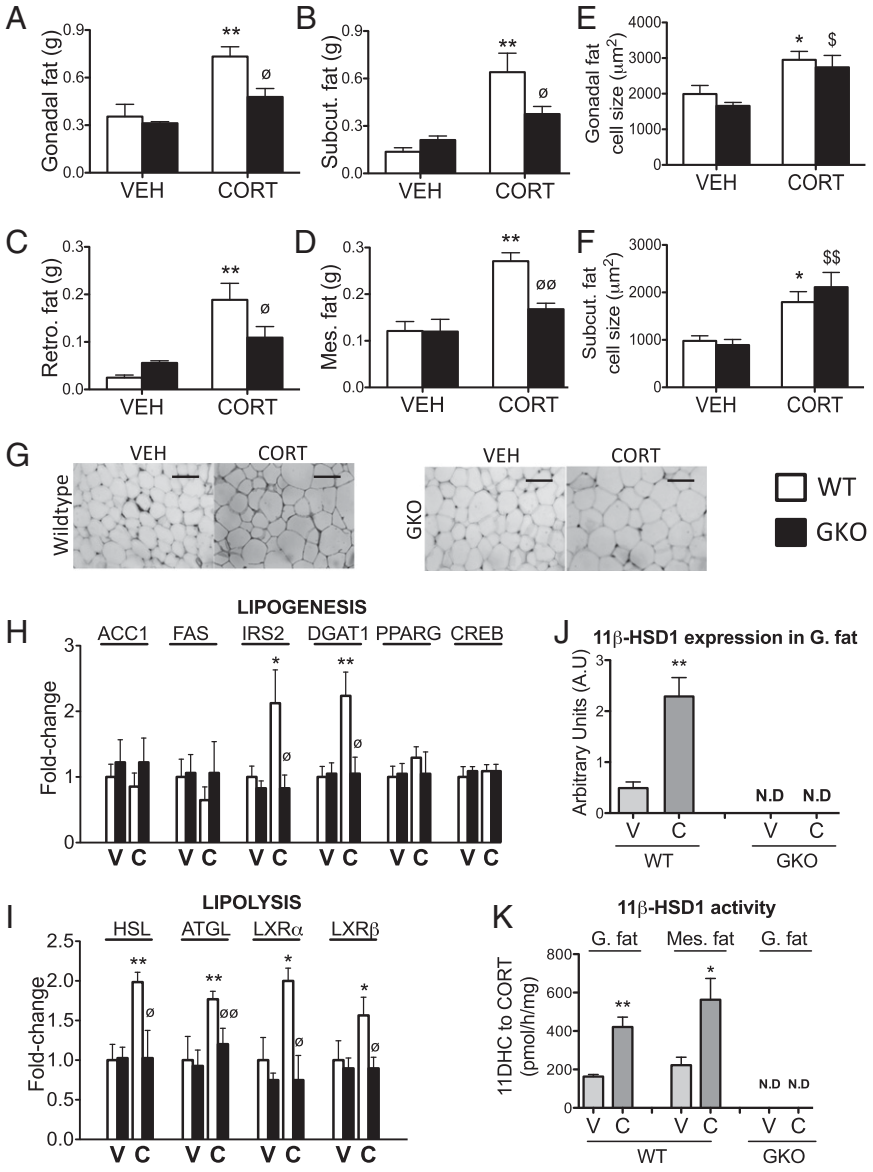


**Fig. 4.** The 11β-HSD1 KO mice are protected from increased adiposity induced by CORT. The 11β-HSD1 KO mice (GKO, black bars) were protected from CORT-mediated increases in gonadal (*A*), s.c. (*B*), retroperitoneal (*C*), and mesenteric (*D*) adiposity compared with CORT-treated WT mice (white bars). H&E staining of paraffin-embedded gonadal fat sections revealed increased adipocyte size in both CORT-treated WT and GKO mice (*E* and *G*). A similar increase in adipocyte size was observed in the s.c. adipose tissue depot (*F*). The mRNA expression of the key lipogenic mediatorsACC1, FAS, PPARG, and CREB was unaffected by CORT treatment in both WT and GKO mice, whereas IRS2 and DGAT1 were increased by CORT in WT mice only (*H*). The mRNA expression of key lipolytic genes was increased in gonadal adipose tissue of CORT-treated WT mice, but not CORT- treated GKOs (*I*). Data were analyzed using two-way ANOVA; see Fig. S3 for the complete dataset used in the analysis. The 11β-HSD1 mRNA expression (*J*) and oxo-reductase activity (*K*) in adipose tissue were increased in CORT-treated WT mice but not GKO mice. Data were analyzed using Student *t* tests ($n = 7$–9 in each group). $^{*}P < 0.05$, $^{**}P < 0.01$ vs. WT vehicle; $^{\varnothing}P < 0.05$, $^{\varnothing\varnothing}P < 0.01$ vs. WT CORT; $^{\$}P < 0.05$, $^{\$\$}P < 0.01$ vs. GKO vehicle. C, CORT; N.D, not detected; V, vehicle. (Scale bars, 100 μm.)

insulin-stimulated lipogenesis. By contrast, CORT-treated GKO mice were protected from increased DGAT1 and IRS2 expression (Fig. 4*H*). The expression of other lipogenic genes including ACC1, FAS, PPARG, and CREB was unaffected by GC treatment in both WT and GKO mice (Fig. 4*H*). Despite increased adiposity, lipid mobilization was elevated in CORT-treated WT mice, with increased expression of the lipolytic enzymes adipose triglyceride lipase (ATGL) and hormone-sensitive lipase (HSL) and increased expression of transcription factors regulating lipolysis, liver X receptor (LXR) α and LXRβ (Fig. 4*I*), paralleled by increased serum fatty acid levels (Fig. 3*C*). By contrast, CORT-treated GKO mice were protected from increased ATGL, HSL, LXRα, and LXRβ expression and increased serum free fatty acids (Figs. 4*I* and 3*C*). The 11β-HSD1 mRNA expression and 11β-HSD1-mediated oxo-reductase activity (conversion of 11DHC to CORT) were increased in the adipose tissue of CORT-treated WT mice compared with vehicle-treated controls. By contrast, no 11β-HSD1 expression or oxo-reductase activity was observed in adipose tissue of either vehicle- or CORT-treated GKO mice (Fig. 4 *J* and *K*).

**Skeletal Muscle.** Skeletal myoatrophy is a key feature of exogenous GC excess; in keeping with this observation, WT mice treated with CORT had decreased grip strength (Fig. 5*A*). This was paralleled by decreased mass of type IIb fiber-rich muscle beds (Fig. 5 *B* and *C*), but not the type I fiber-rich soleus muscles.

Histologically, quadriceps muscles from CORT-treated WT mice had reduced myofiber cross-sectional area, compared with vehicle-treated animals (Fig. 5*D*). Consistent with these observations, increased mRNA expression of several key atrophy markers was observed following CORT treatment in WT mice, including muscle ring finger-1 (MuRF1) and atrogin1 (both E3 ubiquitin ligases) (Fig. 5 *E* and *F*), myostatin (Mstn) (a negative regulator of muscle mass) (Fig. 5*G*), and forkhead box O1 (FoxO1) (a transcription factor that regulates muscle mass) (Fig. 5*H*). GKO mice were protected from the reduced grip strength (Fig. 5*A*), decreased lean mass (Fig. 5 *B* and *C*), and diminished myofiber diameter (Fig. 5*D*) induced by CORT. Furthermore, CORT-mediated induction of muscle atrophy markers MuRF1, atrogin1, Mstn, and FoxO1 were also blunted in GKO animals (Fig. 5 *E*–*H*). The 11β-HSD1 mRNA expression and 11β-HSD1-mediated oxo-reductase activity (conversion of 11DHC to CORT) were increased in quadriceps muscle of CORT-treated WT mice compared with vehicle-treated controls. By contrast, no 11β-HSD1 expression or oxo-reductase activity was observed in quadriceps muscles of either vehicle- or CORT-treated GKO mice (Fig. 5 *I* and *J*).

**Skin.** A reduction in skin thickness is a well-established side effect of GC excess, and we have previously shown 11β-HSD1 to play a central role in age-associated skin thinning (18). CORT dramatically reduced skin thickness in WT mice (Fig. 6*A*), with

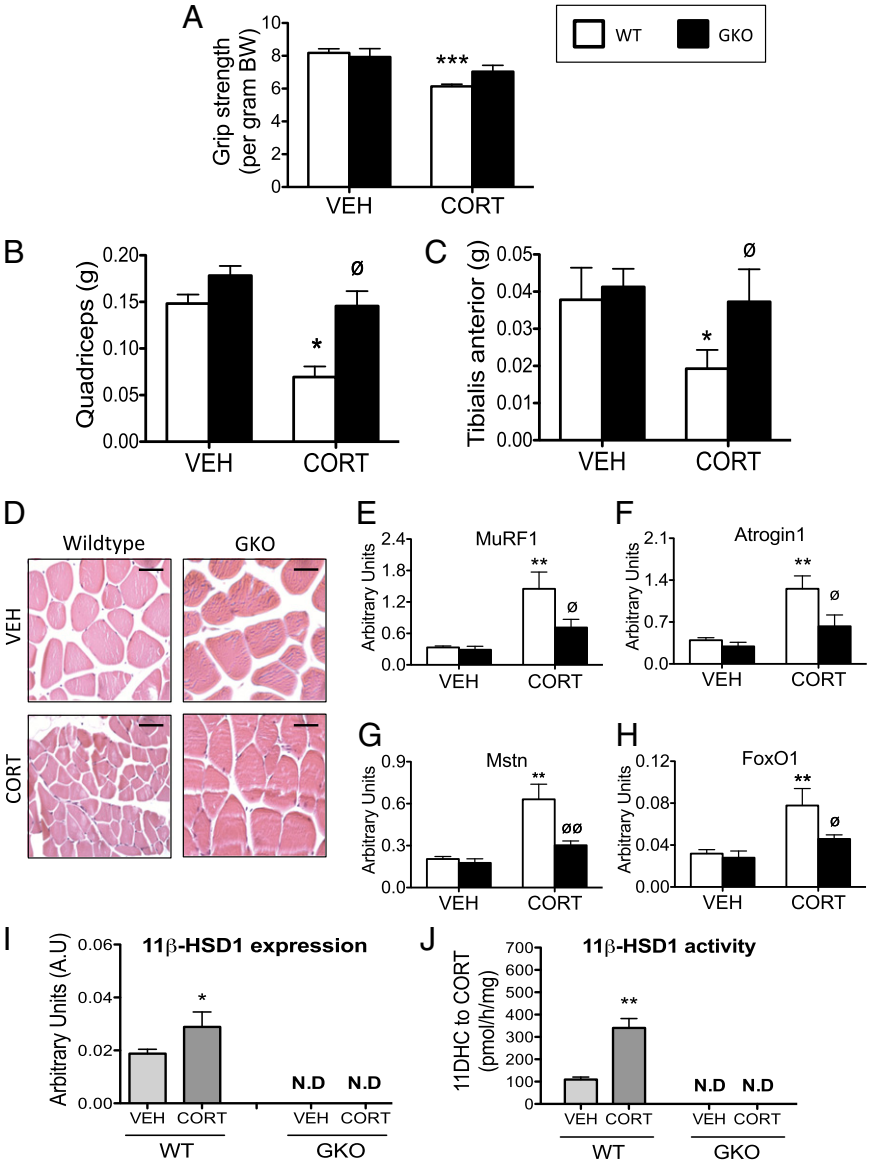


**Fig. 5.** The 11β-HSD1 KO mice are protected from skeletal myopathy induced by CORT. Grip strength (*A*), quadriceps muscle bed weights (*B*), and tibialis anterior muscle bed weights (*C*) were reduced in CORT-treated WT mice (white bars), whereas 11β-HSD1 KO mice (GKO, black bars) were protected from the effects of CORT. Paraffin-embedded quadriceps muscle sections stained with H&E revealed a smaller myofiber diameter in CORT-treated WT mice, whereas CORT was without effect on myofiber diameter in GKO animals (*D*) (Scale bars, 200 μm.) Similarly, GKO mice were protected from the induction of several muscle atrophy markers including MuRF1 (*E*), atrogin-1 (*F*), myostatin (*G*), and FoxO1 (*H*) following CORT treatment. Data were analyzed using two-way ANOVA; see Fig. S4 for the complete dataset used in the analysis. The 11β-HSD1 mRNA expression (*I*) and oxo-reductase activity (*J*) in quadriceps muscle was increased in CORT-treated WT mice but not GKO mice. Data were analyzed using Student *t* tests ($n = 7$–9 in each group). $^{*}P < 0.05$, $^{**}P < 0.01$, $^{***}P < 0.001$ vs. WT vehicle; $^{\varnothing}P < 0.05$ vs. WT CORT. N.D, not detected.

significant atrophy of the collagen-rich dermal layer (Fig. 6*B*). This was accompanied by decreased expression of a number of genes involved in collagen biosynthesis and processing that we have shown to be GC-regulated in skin (18), including collagen 1 (col1a1) (the major structural component of the dermis) (Fig. 6*C*), prolyl hydroxylase (leprel1), and lysyl hydroxylase (PLOD1) (both catalyze the hydroxylation of collagen at proline and lysine residues, respectively, a key step in collagen cross-linking) (Fig. 6 *D* and *E*). The expression of lysyl oxidase (LOX) (catalyses the cross-linking of collagen with elastin) was unchanged following CORT treatment (Fig. 6*F*). By contrast, CORT failed to induce dermal atrophy in GKO mice (Fig. 6 *A* and *B*), with no change in the mRNA expression of Col1A1, Leprel1, and PLOD1 (Fig. 6 *C*–*F*). As with the other tissues investigated in this study, 11β-HSD1 mRNA expression and 11β-HSD1–mediated oxo-reductase activity (conversion of 11DHC to CORT) was increased in the skin of CORT-treated WT mice compared with vehicle-treated controls. By contrast, no 11β-HSD1 expression or oxo-reductase activity was observed in skin of either vehicle- or CORT-treated GKO mice (Fig. 6 *G* and *H*).

As with CORT, 11DHC treatment (which requires activation by 11β-HSD1) in WT mice was effective at elevating circulating CORT levels (Fig. S1*A*) and inducing adrenal atrophy (Fig. S1*B*). Furthermore, 11DHC treatment resulted in a Cushingoid phenotype identical to that observed in CORT-treated WT mice. Specifically, 11DHC treatment induced glucose intolerance (Fig. S1 *C* and *D*), hyperinsulinemia (Fig. S1*E*), systolic hypertension (Fig. S1*F*), hepatic steatosis (Fig. S2 *A* and *B*), elevated serum free fatty acids (Fig. S2*C*), adiposity (Fig. S3 *A*–*F*), increased lipolysis in adipose tissue (Fig. S3*G*), skeletal myopathy (Fig. S4),

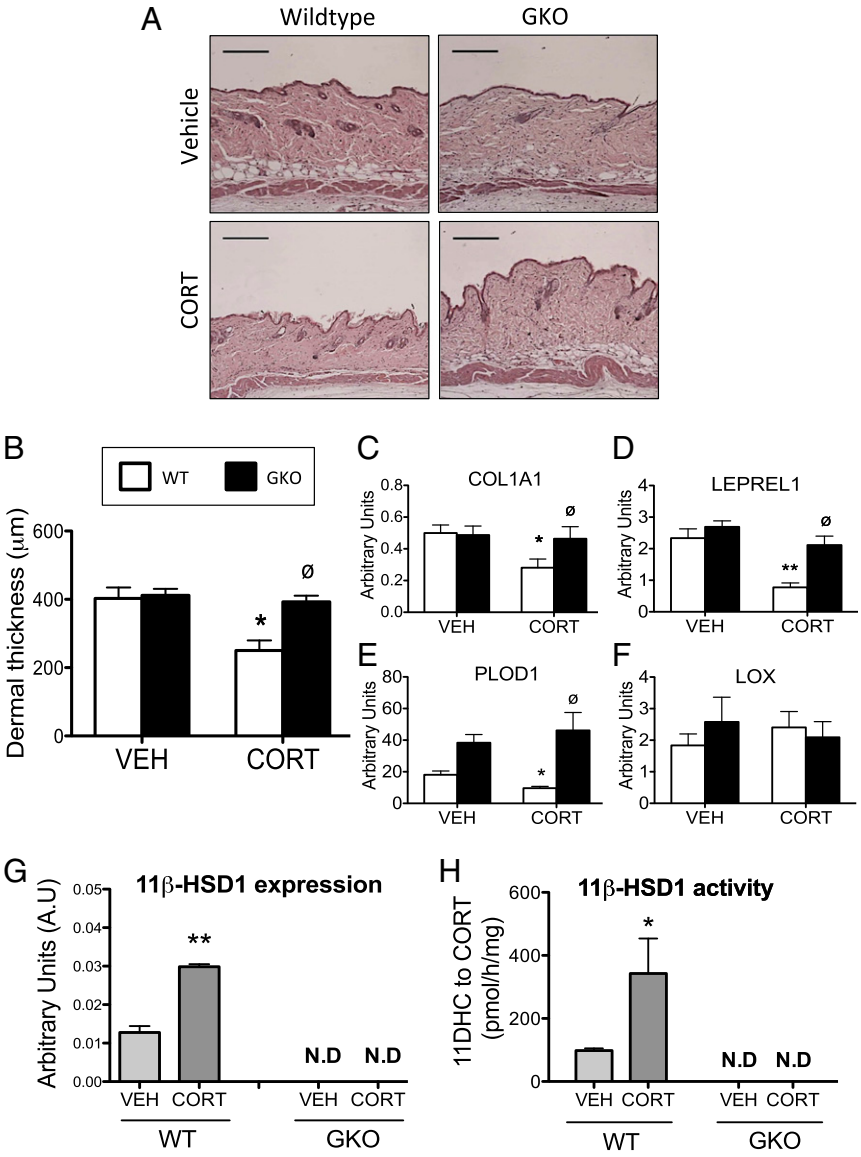


**Fig. 6.** The 11β-HSD1 KO mice are protected from skin thinning induced by CORT. Paraffin-embedded skin sections stained with H&E revealed dramatically reduced skin thickness in WT mice following CORT treatment (*A*). By contrast, CORT was without effect on skin thickness in 11β-HSD1 KO mice (GKO) mice (*A*). (Scale bars, 200 μm.) Dermal thickness was quantified using ImageJ software (*B*). In agreement with the histology, GKO mice were shielded from decreased expression of several genes involved in collagen biosynthesis and processing in skin induced by CORT, including Col1A1 (*C*), Leprel1 (*D*), and PLOD1 (*E*), but not LOX (*F*). $n = 3$ for skin histology and $n = 7$–9 for gene expression and 11β-HSD1 activity data. Data were analyzed using two-way ANOVA; see Fig. S5 for the complete dataset used in the analysis. The 11β-HSD1 mRNA expression (*G*) and oxo-reductase activity (*H*) in skin were increased in CORT-treated WT mice but not GKO mice. Data were analyzed using Student *t* tests. $^{*}P < 0.05$, $^{**}P < 0.01$ vs. WT vehicle; $^{\varnothing}P < 0.05$ vs. WT CORT. N.D, not detected.

and dermal atrophy (Fig. S5). As anticipated, 11DHC-treated GKO mice were indistinguishable from vehicle-treated animals for all parameters assessed.

**Deletion of 11β-HSD1 in Adipose Tissue, but Not the Liver, Protects from the Hepatic Manifestation of GC-Induced Cushing Syndrome.** To test whether GCs, reactivated by 11β-HSD1 in the liver and/or adipose tissue, contribute to the adverse effects of GC excess, we treated liver- and adipose-specific 11β-HSD1 KO mice (LKO and FKO, respectively) with CORT (100 μg/mL), 11DHC (100 μg/mL), or vehicle via drinking water for 5 wk. Details with respect to the generation of these transgenic lines are presented in ref. 19, *SI Text*, and Fig. S6 *A–E*.

In contrast to GKO mice, neither FKO nor LKO mice were protected from increased adiposity, decreased lean mass (Tables S1 and S2), glucose intolerance (Figs. S7 *A–C* and S8 *A–C*), hyperinsulinemia (Figs. S7*D* and S8*D*), or reduced grip strength (Figs. S7*E* and S8*E*) following CORT or 11DHC treatment.

Similarly, LKO mice were not protected from increased hepatic TAG accumulation (Fig. 7 *A* and *B* and Fig. S9 *A* and *B*), increased serum free fatty acids (Fig. 7*C* and Fig. S9*C*), or increased adipose expression of HSL, ATGL, LXRα, LXRβ (Fig. S9*D*) or hepatic CD36 (Fig. S9*E*) following CORT or 11DHC treatment. Surprisingly, the magnitude of response observed in the 11DHC-treated LKO mice was similar to that of the 11DHC-treated control animals, suggesting extrahepatic 11β-HSD1 activity is mostly responsible for mediating the effects of 11DHC in this study.

FKO mice were, however, significantly protected from both CORT- and 11DHC-induced hepatic TAG accumulation (Fig. 7 *A* and *B* and Fig. S10 *A* and *B*), increased serum free fatty acids

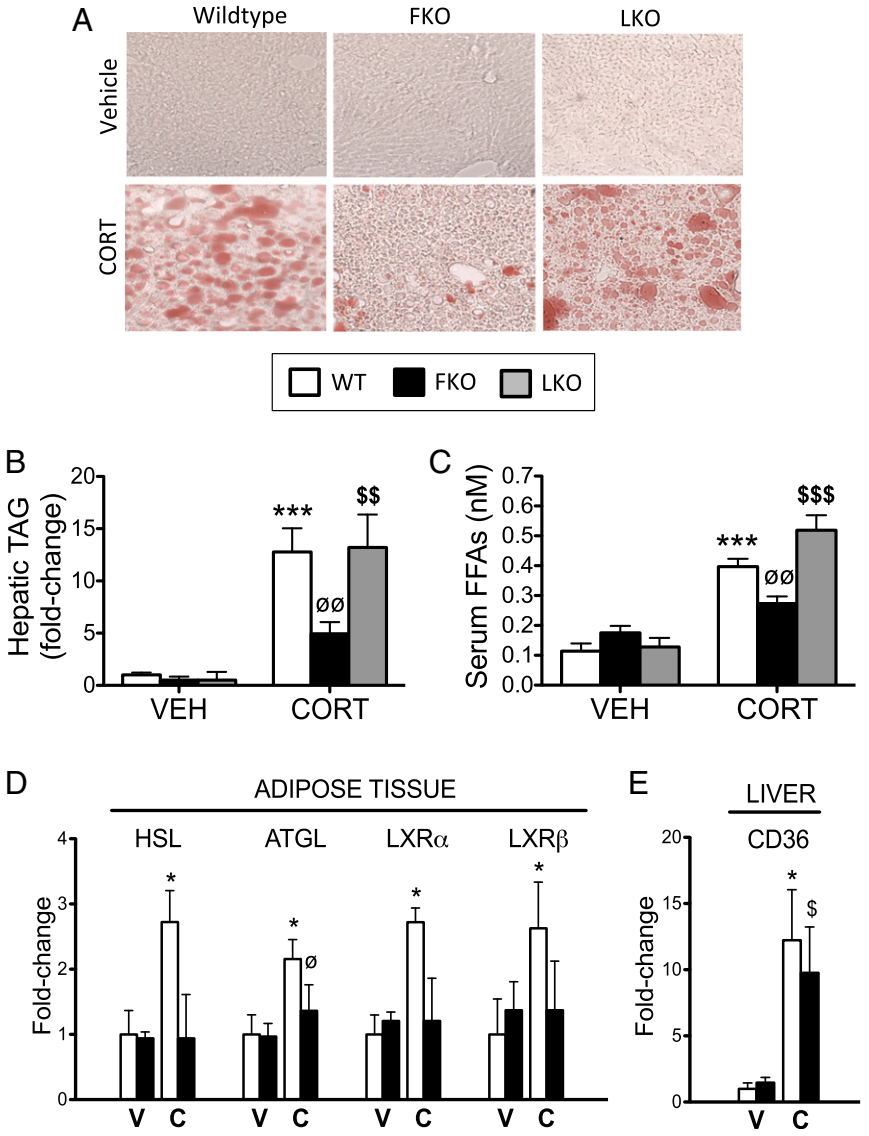


**Fig. 7.** Fat-specific 11β-HSD1 KO mice, and not liver-specific 11β-HSD1 KO mice, are protected from the development of CORT-induced hepatic steatosis. Frozen liver sections stained with oil red O (*A*) and hepatic TAG quantification (*B*) revealed adipose-specific 11β-HSD1 KO mice (FKO, black bars), and not liver-specific 11β-HSD1 KO mice (LKO, gray bars), were protected from CORT-induced hepatic steatosis, compared with CORT-treated WT controls (white bars). Similarly, FKO mice (and not LKO mice) were shielded from increased serum free fatty acids (*C*) and increased mRNA expression of key lipolytic mediators in adipose tissue (*D*) following CORT treatment. FKO mice were not protected from increased expression of the hepatic free fatty acid transporter CD36 induced by CORT in WT mice (*E*). Data were analyzed using two-way ANOVA; see Figs. S9 and S10 for the complete datasets used in the analysis ($n$ = 6–7 in each group). $^{*}P < 0.05$, $^{***}P < 0.001$ vs. WT vehicle; $^{\varnothing}P < 0.05$, $^{\varnothing\varnothing}P < 0.01$ vs. WT CORT; $^{\$}P < 0.05$, $^{\$\$}P < 0.01$, $^{\$\$\$}P < 0.001$ vs. LKO vehicle. C, CORT; V, vehicle.

(Fig. 7*C* and Fig. S10*C*), and increased adipose expression of HSL, ATGL, LXRα, and LXRβ (Fig. 7*D* and Fig. S10*D*), but not increased hepatic CD36 expression (Fig. 7*E* and Fig. S10*E*). Although in the case of LXRα and LXRβ the difference between GC-treated FKO and GC-treated controls did not reach statistical significance, the ability of CORT and 11DHC to up-regulate these genes was clearly attenuated in the FKO mice. Taken together, these data suggest intracellular GC availability in adipose tissue, and not the liver, underpins hepatic TAG accumulation following exogenous GC treatment in WT mice.

## Discussion

Since the discovery of cortisone in 1950, and demonstration of its potent anti-inflammatory effect in patients with rheumatoid arthritis (Nobel laureates Hench, Kendall, and Reichstein), prescribed GCs are widely used throughout medicine as potent anti-inflammatory and immunosuppressive agents. However, they cause side effects, as predicted from the phenotype of patients with endogenous Cushing syndrome, that contribute to increased cardiovascular risk (3–5). Here we demonstrate that the reactivation of GCs by 11β-HSD1 in peripheral tissues, in contrast to circulating levels, is a major determinant of the phenotype of GC excess in mice, and when deleted the metabolic side effects associated with GC excess are ameliorated. Our data challenge the idea that simple delivery of active GCs from the circulation represents the most important level of regulation of GC action. As such, 11β-HSD1 may be a novel target for therapeutic intervention in patients with Cushing syndrome, as well as offering a possible strategy to limit the adverse effects of prescribed GCs.

Our data suggest that exogenously administered CORT may contribute to GR activation by three different mechanisms (Fig. 1*C*). First, circulating CORT can enter the cell and bind/activate cytoplasmic glucocorticoid receptor (GR) directly. Second, CORT may be inactivated to 11DHC by 11β-HSD2, largely in the kidneys, and once delivered to key metabolic target tissues is reactivated to CORT by 11β-HSD1 to allow GR activation. In agreement, elevated urinary cortisone levels (the inactive precursor of cortisol and the human equivalent of 11DHC) have been reported in patients diagnosed with endogenous/exogenous Cushing syndrome and Cushing disease (20). Third, GR activation stimulates 11β-HSD1 expression and activity, further fueling GC excess. This feed-forward action has previously been demonstrated in both in vitro and in vivo studies (15, 21–23). Physiologically, an acute increase in local GC availability is important in rapidly resolving local inflammation. However, if 11β-HSD1 activity remains chronically elevated, the consequences are likely to be less beneficial, and this could contribute to the phenotype of GC excess. Indeed, forced overexpression of 11β-HSD1 in adipose tissue and liver in mice results in features of metabolic disease, without elevating circulating GC levels (9–11).

Our data highlight a potentially critical role for cortisone in the phenotype of GC excess and raise an intriguing question: Is Cushing a cortisone disease? Importantly, cortisone has limited binding to corticosteroid-binding globulin in the circulation and no circadian rhythm, in contrast to cortisol. Therefore, for the most part, free cortisone levels will exceed those of free, unbound cortisol, resulting in an abundance of substrate for 11β-HSD1 in peripheral tissues. This concept makes physiological sense, in terms of individual tissues regulating precisely their GC availability—rather than its being dictated by a distant gland. Indeed, circulating cortisone levels have been shown to be negatively associated with bone mineral density and osteocalcin levels independent of circulating cortisol levels, suggesting 11β-HSD1 activity within osteoblasts regulates bone mineral density (24).

These observations are likely to be most applicable to patients prescribed GCs with kinetics similar to those of endogenous cortisol. Interestingly, prednisolone in most of the United Kingdom and Europe, and prednisone in the United States, are currently the most widely prescribed synthetic GC and are metabolized by 11β-HSDs 1 and 2 in a totally analogous fashion to cortisol and cortisone, with similar kinetic affinities (25). Because this inactivation/reactivation loop has the potential to increase intracellular prednisolone levels, this mechanism may be central to the adverse systemic side-effect profile associated with these commonly prescribed steroids.

In an effort to pinpoint which 11β-HSD1–expressing tissue(s) are involved in driving the metabolic side effects associated with GC excess, we examined the impact of GC administered to mice with targeted deletions of 11β-HSD1 in adipose tissue and liver. We demonstrated that GC-treated adipose-specific 11β-HSD1 KO mice are protected from hepatic TAG accumulation, increased serum free fatty acids, and increased expression of adipose lipolytic enzymes, but protection from increased expression of the fatty acid transporter in the liver, CD36, was not observed—suggesting hepatic fatty acid uptake is unaffected by deletion of 11β-HSD1 in adipose tissue. This may offer an explanation as to why protection from GC-induced hepatic TAG accumulation did not totally revert to that in vehicle-treated levels.

In contrast, liver-specific 11β-HSD1 KO animals were not protected from any of these GC-dependent affects. This strongly suggests increased intracellular GC availability in adipose tissue, and not the liver, underpins hepatic TAG accumulation in GC-treated WT mice. In support, GCs are well known to directly stimulate lipolysis in adipose tissue, resulting in elevated serum free fatty acid levels (26). However, we have not fully discounted the possibility that increased GC delivery from adipose tissue to the liver via the portal vein underpins these phenotypic observations. The fact that neither adipose-specific nor liver-specific 11β-HSD1 KO mice were protected from glucose intolerance, hyperinsulinemia, decreased lean mass, and increased adiposity following exogenous GC treatment is likely to reflect the importance of GCs reactivated by 11β-HSD1 in tissues other than the liver and adipose tissue, such as skeletal muscle.

In contrast to our findings, Harno et al. (14) recently demonstrated that liver-specific 11β-HSD1 KO mice were protected from glucose intolerance, hyperinsulinemia, and increased adiposity induced by low-dose 11DHC administered orally, although the effects of CORT treatment was not explored. The studies differed in the doses of 11DHC used, and it may be that deletion of hepatic 11β-HSD1 offers some protection from the mild side effects associated with low-dose inactive GC administration. However, we have demonstrated that at a higher dose GCs reactivated by 11β-HSD1 in extrahepatic tissues play a major role in driving a florid Cushing phenotype, suggesting first-pass metabolism is not the sole regenerator of orally administered inactive GCs.

Our data suggest that therapeutically targeting 11β-HSD1, either locally (in the case of skin thinning) or systemically (in the case of the other metabolic features), may offer a novel adjunctive therapy to limit the side-effect profile associated with exogenous GC treatment and endogenous Cushing syndrome/disease. Importantly, we have shown that the 11β-HSD1 KO mice cannot activate 11DHC to CORT following vehicle or CORT treatment in a number of key metabolic tissues, suggesting no alternative reductase is capable of compensating for loss of 11β-HSD1 activity. Because adipose-specific 11β-HSD1 KO mice are partially protected from exogenous Cushing syndrome, 11β-HSD1 expressed in adipose tissue would need to be the primary target of these compounds. However, selectively inhibiting 11β-HSD1 may not offer complete protection from the phenotype of GC excess, because the ability of GCs to bind the GR directly would be unaffected. Preclinical and clinical studies have shown selective 11β-HSD1 inhibitors to improve insulin sensitivity, reduce dyslipidemia, and reverse central obesity in patients with type 2 diabetes (12, 13). Furthermore, we have recently demonstrated that 11β-HSD1 blockade prevents age- and

photosensitivity-induced skin structure and function defects (18). Although these compounds are still being evaluated clinically, their potential to block the adverse side-effect profile associated with GC excess is an exciting prospect. However, despite the fact that these compounds seem to be well tolerated in short-term studies, the consequences of long-term 11β-HSD1 suppression in humans is unknown, and further studies are necessary to ensure that symptoms suggestive of tissue-specific GC deficiency are not encountered.

Importantly, the adverse metabolic complications associated with GC excess involve the key metabolic tissues, liver, adipose tissue, and skeletal muscle, which have comparatively high 11β-HSD1 activity. As such, administering a selective 11β-HSD1 inhibitor under conditions of GC excess is likely to have its greatest impact in these tissues.

Current strategies used to abrogate Cushingoid features include the recently licensed use of the GR antagonist Mifepristone (27). The development of selective GR agonists (28) that target the transrepressive effects of GCs over the tranasctivating actions looks promising (29, 30) but a clinical drug has not yet been delivered. Numerous selective 11β-HSD1 inhibitors have been developed and many tested in phase II studies (12, 13); their evaluation in patients with Cushing syndrome will be of great interest.

In summary, we have shown that GCs, reactivated by 11β-HSD1 in peripheral tissues, are major determinants of exogenous Cushing syndrome in mice and, when deleted, the metabolic Cushingoid side effects associated with GC excess are ameliorated, despite elevated circulating concentrations. Furthermore, we have demonstrated that local GC regeneration in adipose tissue is central in driving the hepatic manifestations of GC excess. Taken together, this raises the intriguing possibility of using selective 11β-HSD1 inhibitors as an adjunctive therapy to limit the side effects associated with GC excess in endogenous and exogenous Cushing syndrome.

## Research Design and Methods

**Administration of GCs in Vivo.** All procedures were carried out in accordance with the UK Animals (Scientific Procedures) Act 1986. Six-week-old male global (GKO) (C57BL/6) (31), liver-specific (LKO) (C57BL/6J/129SvJ) (19), and adipose-specific (FKO) C57BL/6J (*SI Text*) 11β-HSD1 KO mice, with WT controls, had ad libitum access to standard chow and drinking water supplemented with either CORT (100 μg/mL, 0.66% ethanol), 11DHC (100 μg/mL, 0.66% ethanol), or vehicle (0.66% ethanol) for 5 wk. Treatments were replaced twice weekly. At the end of the experiment, animals were culled by cervical dislocation and tissues excised, weighed, and snap-frozen using liquid nitrogen for later analyses.

**Metabolic Assessments.** Glucose tolerance was assessed during week 4 by fasting mice 5 h before blood glucose was measured from tail vein nicks using a glucometer (Accu-Chek; Roche) at 0, 15, 30, 60, 90, and 120 min after glucose i.p. injection (2 g/kg). A blood sample was taken at baseline for insulin determination, measured using the Ultra Sensitive Mouse Insulin ELISA kit (Crystal Chem, Inc.). An insulin resistance score (HOMA-IR) was calculated with the following formula: fasting plasma glucose (millimolar) × fasting serum insulin (microunits per liter) divided by 22.5. Low HOMA-IR values indicate high insulin sensitivity, whereas high HOMA-IR values indicate low insulin sensitivity (insulin resistance). Grip strength was assessed during week 4 using a digital grip-strength meter (Linton Instrumentation). Each mouse underwent four repeat readings before results were averaged and normalized to body weight.

**Blood Pressure Assessment.** Using a separate cohort from those used for metabolic assessments, blood pressure was measured using tail cuff plethysmography according to the manufacturer's instructions (BP-2000 Blood Pressure Analysis System; Visitech Systems). Briefly, mice were restrained and tail cuffs with pneumatic pulse sensors attached to tails. Mice were habituated to this procedure for 10 d before measurements were recorded. Results presented are averaged systolic blood pressure measurements taken over the final 7 d of the 5-wk treatment period.

**Hepatic TAG Quantification.** Hepatic TAG content was measured using a colorimetric assay according to the manufacturer's instructions (BioVision, Inc.). Samples were prepared by homogenizing 100 mg of liver tissue in 1 mL of 5% Nonidet P-40 in water; samples were heated to 80–100 °C in a water bath for 2–5 min and then allowed to cool to room temperature. The heating step was repeated to solubilize all TAGs, upon which samples were centrifuged for 2 min to remove any insoluble material. Samples were diluted 10-fold with distilled $H_2O$ before being subjected to a TAG assay.

**Serum CORT and Free Fatty Acid Quantification.** Mouse blood was obtained by cardiac puncture and immediately centrifuged at 1,000 × *g* in heparin-coated tubes. Serum was transferred to cryotubes and snap-frozen. CORT and free fatty acid levels were measured according to the manufacturer's instructions (Abcam plc and BioVision, Inc., respectively).

**Tissue Histology and Oil Red O Staining.** Quadriceps muscle, gonadal adipose tissue, and skin were fixed in 4% (vol/vol) buffered paraformaldehyde. Samples were subsequently paraffin-embedded and 8-μm sections prepared on a microtome (Leica). Sections were stained with hematoxylin and eosin, and adipocyte area and skin thickness (dermal layer) were quantified using ImageJ software. Frozen liver samples were embedded in optimal cutting temperature reagent (Tissue-Tek; Sakura Finetek) and sectioned at 8 μm on a cryostat (Leica). Cryosections were fixed in formaldehyde before incubation in 0.5% oil red O in isopropyl alcohol. After rinsing in distilled water, liver sections were mounted with permanent aqueous mounting medium Gel/Mount (Biomeda) and photographed using light microscopy.

**11β-HSD1 Enzyme Assays in Tissue Explants.** Mouse tissue was obtained as detailed above, oxo-reductase activity (11DHC to CORT) was assessed by incubating freshly dissected tissue explants with 100 nm 11DHC diluted in 1 mL media (in glass tubes) with tracer amounts of [$^3$H]11DHC (synthesized in-house) (32) at 37 °C for 2 h. Following incubation, steroids were extracted from the medium with dichloromethane, separated by TLC with chloroform/ethanol (92:8), and the fractional conversion of steroids was calculated by scanning analysis with a Bioscan 2000 radioimaging detector (Bioscan). Percentage conversion was normalized to tissue weight.

**RNA Extraction and Real-Time PCR.** Total RNA was extracted from tissue and cells using the Tri-Reagent system. RNA integrity was assessed by electrophoresis on 1% agarose gel. Concentration was determined spectrophotometrically at $OD_{260}$. In a 50-μL volume, 500 ng of total RNA was incubated with 250 μM random hexamers, 500 μM dNTPs, 20 U RNase inhibitor, 63 U Multiscribe reverse transcriptase, 5.5 mM MgCl, and 1× reaction buffer. The reverse transcription reaction was carried out at 25 °C for 10 min and at 48 °C for 30 min before the reaction was terminated by heating to 95 °C for 5 min. mRNA levels were determined using an ABI 7500 sequence detection system (Applied Biosystems). Reactions were performed in singleplex in 10-μL volumes on 96-well plates in reaction buffer containing 2× TaqMan Universal PCR Master Mix (Applied Biosystems). Primers and probes were supplied by Applied Biosystems as premade "assay on demands." All reactions were normalized against the housekeeping gene 18S rRNA, provided as a pre-optimized control probe. All target genes were labeled with FAM and the reference gene with VIC. The reaction conditions were as follows: 95 °C for 10 min, then 40 cycles of 95 °C for 15 s and 60 °C for 1 min. Data were obtained as Ct values (cycle number at which logarithmic PCR plots cross a calculated threshold line) and used to determine ΔCt values [(Ct of the target gene) – (Ct of the reference gene)]. Data were expressed as arbitrary units using the following transformation: [arbitrary units (AU) = $1{,}000 \times (2^{-\Delta Ct})$]. When used, fold changes were calculated using the following equation: [fold increase = $2^{-\text{difference in } \Delta Ct}$].

**Statistical Analysis.** Statistical comparisons were performed using SigmaStat 3.1 (Systat Software, Inc.). Data are presented as mean ± SEM with statistical significance defined as $P < 0.05$. Two-way ANOVA followed by Bonferroni's multiple comparison post hoc test was used to compare treatments and genotypes. Statistical analysis on real-time PCR data were performed on ΔCt values and not fold changes or AU.

**ACKNOWLEDGMENTS.** We thank Lianne Abrahams (School of Clinical and Experimental Medicine, University of Birmingham) for technical support. This work was supported by Medical Research Council Senior Clinical Fellowship G0802765 (to J.W.T.), Wellcome Trust Program Grant 082809 (to P.M.S.), Biotechnology and Biomedical Sciences Research Council Grants BB/G023468/1 (to G.G.L.) and BBB/S/M/2006/13045 (to S.A.M.), and a European Research Council Advanced Research Fellowship (to P.M.S.).

1. van Staa TP, et al. (2000) Use of oral corticosteroids in the United Kingdom. *QJM* 93(2):105–111.
2. Overman RA, Yeh JY, Deal CL (2013) Prevalence of oral glucocorticoid usage in the United States: A general population perspective. *Arthritis Care Res (Hoboken)* 65(2): 294–298.
3. Fardet L, et al. (2007) Corticosteroid-induced clinical adverse events: Frequency, risk factors and patient's opinion. *Br J Dermatol* 157(1):142–148.
4. Fardet L, Petersen I, Nazareth I (2012) Risk of cardiovascular events in people prescribed glucocorticoids with iatrogenic Cushing's syndrome: Cohort study. *BMJ* 345: e4928.
5. Wei L, MacDonald TM, Walker BR (2004) Taking glucocorticoids by prescription is associated with subsequent cardiovascular disease. *Ann Intern Med* 141(10):764–770.
6. Hassan-Smith ZK, et al. (2012) Outcome of Cushing's disease following transsphenoidal surgery in a single center over 20 years. *J Clin Endocrinol Metab* 97(4): 1194–1201.
7. Cushing H (1932) The basophil adenomas of the pituitary body and their clinical manifestations (pituitary basophilism). *Bull Johns Hopkins Hosp* 50:137–195.
8. Morgan SA, et al. (2009) 11beta-hydroxysteroid dehydrogenase type 1 regulates glucocorticoid-induced insulin resistance in skeletal muscle. *Diabetes* 58(11): 2506–2515.
9. Masuzaki H, et al. (2001) A transgenic model of visceral obesity and the metabolic syndrome. *Science* 294(5549):2166–2170.
10. Masuzaki H, et al. (2003) Transgenic amplification of glucocorticoid action in adipose tissue causes high blood pressure in mice. *J Clin Invest* 112(1):83–90.
11. Paterson JM, et al. (2004) Metabolic syndrome without obesity: Hepatic overexpression of 11beta-hydroxysteroid dehydrogenase type 1 in transgenic mice. *Proc Natl Acad Sci USA* 101(18):7088–7093.
12. Feig PU, et al. (2011) Effects of an 11β-hydroxysteroid dehydrogenase type 1 inhibitor, MK-0916, in patients with type 2 diabetes mellitus and metabolic syndrome. *Diabetes Obes Metab* 13(6):498–504.
13. Rosenstock J, et al.; INCB13739-202 Principal Investigators (2010) The 11-beta-hydroxysteroid dehydrogenase type 1 inhibitor INCB13739 improves hyperglycemia in patients with type 2 diabetes inadequately controlled by metformin monotherapy. *Diabetes Care* 33(7):1516–1522.
14. Harno E, et al. (2013) 11-Dehydrocorticosterone causes metabolic syndrome, which is prevented when 11β-HSD1 is knocked out in livers of male mice. *Endocrinology* 154(10):3599–3609.
15. Yang C, et al. (2011) 5α-reduced glucocorticoids exhibit dissociated anti-inflammatory and metabolic effects. *Br J Pharmacol* 164(6):1661–1671.
16. Karatsoreos IN, et al. (2010) Endocrine and physiological changes in response to chronic corticosterone: a potential model of the metabolic syndrome in mouse. *Endocrinology* 151(5):2117–2127.
17. Tomlinson JW, et al. (2002) Absence of Cushingoid phenotype in a patient with Cushing's disease due to defective cortisone to cortisol conversion. *J Clin Endocrinol Metab* 87(1):57–62.
18. Tiganescu A, et al. (2013) 11β-Hydroxysteroid dehydrogenase blockade prevents age-induced skin structure and function defects. *J Clin Invest* 123(7):3051–3060.
19. Lavery GG, et al. (2012) Lack of significant metabolic abnormalities in mice with liver-specific disruption of 11β-hydroxysteroid dehydrogenase type 1. *Endocrinology* 153(7):3236–3248.
20. Lin CL, Wu TJ, Machacek DA, Jiang NS, Kao PC (1997) Urinary free cortisol and cortisone determined by high performance liquid chromatography in the diagnosis of Cushing's syndrome. *J Clin Endocrinol Metab* 82(1):151–155.
21. Tomlinson JW, Sinha B, Bujalska I, Hewison M, Stewart PM (2002) Expression of 11beta-hydroxysteroid dehydrogenase type 1 in adipose tissue is not increased in human obesity. *J Clin Endocrinol Metab* 87(12):5630–5635.
22. Cooper MS, et al. (2002) Osteoblastic 11beta-hydroxysteroid dehydrogenase type 1 activity increases with age and glucocorticoid exposure. *J Bone Miner Res* 17(6): 979–986.
23. Tiganescu A, Walker EA, Hardy RS, Mayes AE, Stewart PM (2011) Localization, age- and site-dependent expression, and regulation of 11β-hydroxysteroid dehydrogenase type 1 in skin. *J Invest Dermatol* 131(1):30–36.
24. Cooper MS, et al. (2005) Circulating cortisone levels are associated with biochemical markers of bone formation and lumbar spine BMD: The Hertfordshire Cohort Study. *Clin Endocrinol (Oxf)* 62(6):692–697.
25. Meikle AW, Weed JA, Tyler FH (1975) Kinetics and interconversion of prednisolone and prednisone studied with new radioimmunogassays. *J Clin Endocrinol Metab* 41(4):717–721.
26. Xu C, et al. (2009) Direct effect of glucocorticoids on lipolysis in adipocytes. *Mol Endocrinol* 23(8):1161–1170.
27. Fleseriu M, et al.; SEISMIC Study Investigators (2012) Mifepristone, a glucocorticoid receptor antagonist, produces clinical and metabolic benefits in patients with Cushing's syndrome. *J Clin Endocrinol Metab* 97(6):2039–2049.
28. Schäcke H, et al. (2004) Dissociation of transactivation from transrepression by a selective glucocorticoid receptor agonist leads to separation of therapeutic effects from side effects. *Proc Natl Acad Sci USA* 101(1):227–232.
29. Lin CW, et al. (2002) trans-Activation and repression properties of the novel non-steroid glucocorticoid receptor ligand 2,5-dihydro-9-hydroxy-10-methoxy-2,2,4-trimethyl-5-(1-methylcyclohexen-3-y1)-1H-[1]benzopyrano[3,4-f]quinoline (A276575) and its four stereoisomers. *Mol Pharmacol* 62(2):297–303.
30. Zhang JZ, et al. (2009) BOL-303242-X, a novel selective glucocorticoid receptor agonist, with full anti-inflammatory properties in human ocular cells. *Mol Vis* 15: 2606–2616.
31. Semjonous NM, et al. (2011) Hexose-6-phosphate dehydrogenase contributes to skeletal muscle homeostasis independent of 11β-hydroxysteroid dehydrogenase type 1. *Endocrinology* 152(1):93–102.
32. Bujalska IJ, Walker EA, Tomlinson JW, Hewison M, Stewart PM (2002) 11Beta-hydroxysteroid dehydrogenase type 1 in differentiating omental human preadipocytes: from de-activation to generation of cortisol. *Endocr Res* 28(4):449–461.